Published in final edited form as:
J Biomech. 2011 January 4; 44(1): 164–169. doi:10.1016/j.jbiomech.2010.09.003.

Effects of shear stress cultivation on cell membrane disruption and intracellular calcium concentration in sonoporation of endothelial cells

Juyoung Park, **Zhenzhen Fan**, and **Cheri X. Deng***
Department of Biomedical Engineering, University of Michigan, Ann Arbor, Michigan, USA

Abstract

Microbubble facilitated ultrasound (US) application can enhance intracellular delivery of drugs and genes in endothelial cells cultured in static condition by transiently disrupting the cell membrane, or sonoporation. However, endothelial cells *in vivo* that are constantly exposed to blood flow may exhibit different sonoporation characteristics. This study investigates the effects of shear stress cultivation on sonoporation of endothelial cells in terms of membrane disruption and changes in the intracellular calcium concentration ($[Ca^{2+}]_i$). Sonoporation experiments were conducted using murine brain microvascular endothelial (bEnd.3) cells and human umbilical vein endothelial cells (HUVECs) cultured under static or shear stress (5 dyne/cm^2 for 5 days) condition in a microchannel environment. The cells were exposed to a short US tone burst (1.25 MHz, 8 μs duration, 0.24 MPa) in the presence of Definity™ microbubbles to facilitate sonoporation. Membrane disruption was assessed by propidium iodide (PI) and changes in $[Ca^{2+}]_i$ measured by fura-2AM. Results from this study show that shear stress cultivation significantly reduced the impact of ultrasound-driven microbubbles activities on endothelial cells. Cells cultured under shear stress condition exhibited much lower percentage with membrane disruption and changes in $[Ca^{2+}]_i$ compared to statically cultured cells. The maximum increases of PI uptake and $[Ca^{2+}]_i$ were also significantly lower in the shear stress cultured cells. In addition, the extent of $[Ca^{2+}]_i$ waves in shear cultured HUVECs was reduced compared to the statically cultured cells.

Keywords

Endothelial cells; Shear stress; Sonoporation; Ultrasound; Microbubbles

1. Introduction

A gas-filled microbubble undergoes rapid cyclic volume changes and collapse, responding to the oscillatory positive and negative pressures of an ultrasound (US) field. Such microbubble dynamic activities generate local fluid microstreaming, shear stress, and high speed fluid micro-jet that can exert significant mechanical impact to a nearby cell (Ohl et al.,

*Corresponding author: Cheri X. Deng, Department of Biomedical Engineering, University of Michigan, 2200 Bonisteel Blvd, Ann Arbor, MI 48109–2099, USA. Tel: +1 734-936-2855; Fax: +1 734-936-1905. cxdeng@umich.edu..

Conflict of interest statement
The authors have no conflict of interests that could inappropriately influence this article.

2006; Postema et al., 2004; Prentice et al., 2005; van Wamel et al., 2006; VanBavel, 2007; Wu, 2007), leading to disruption of the cell membrane, or sonoporation. Sonoporation effectively increases the cell membrane permeability, thereby allowing transport of impermeable therapeutic agents into the cells (Fan et al., 2010; Kudo et al., 2009; Mayer et al., 2008; van Wamel et al., 2006).

Endothelial cells lining the inside of the blood vessel walls are targets for treating many vascular diseases. *In vitro* studies using statically cultured endothelial cells have shown the feasibility of sonoporation as a promising non-viral strategy to deliver drugs and genes into these cells (Kudo et al., 2009; Lionetti et al., 2009; van Wamel et al., 2006). Bioeffects including the spatiotemporal changes of intracellular calcium concentration ($[Ca^{2+}]_i$), or calcium transients, are also generated in sonoporation (Fan et al., 2010; Juffermans et al., 2006; Kumon et al., 2009; Kumon et al., 2007; Tsukamoto et al., 2008). Such downstream effects could have significant implications because the important roles $[Ca^{2+}]_i$ play in various endothelial physiology and functions. For example, regulation of $[Ca^{2+}]_i$ is involved in the disruption of endothelial cell tight junctions and the blood brain barrier permeability (Abbott, 1998; Bradbury, 1993; Brown and Davis, 2002; Hariri, 1994; Olesen, 1989). Increased $[Ca^{2+}]_i$ is also recognized to activate rapid and prolonged endocytosis (Eliasson et al., 1996; MacDonald et al., 2005) as well as endothelial nitric oxide synthase, which may cause vasodilatation *in vivo* (VanBavel, 2007).

To better recognize the relevance of *in vitro* results, it is important to note that endothelial cells *in vivo* are exposed to blood flow and their properties are greatly influenced by the hemodynamic effects (Garcia-Cardena et al., 2001). Shear stress on endothelial cells induces extended F-actin stress fibers formation in the direction of flow (Girard and Nerem, 1995; Langille et al., 1991; Malek and Izumo, 1996) and causes cell flattening (Barbee et al., 1994). Shear stress also alters gene expression (Morita et al., 1993), stimulates cell adhesion to the substratum (Dardik et al., 1999), and generates dramatic increase in cytoplamsic viscosity and cell membrane rigidity (Lee et al., 2006). These biomechanical adaptation may greatly influence how *in vivo* endothelial cells respond to additional physical or mechanical impacts generated by US-driven microbubble activities in sonoporation (Ohl et al., 2006; Postema et al., 2004; Prentice et al., 2005; van Wamel et al., 2006; VanBavel, 2007; Wu, 2007).

Hence the goal of this study is to investigate the effects of shear stress cultivation on sonoporation using representative endothelial cell lines in terms of membrane disruption and $[Ca^{2+}]_i$ dynamics.

2. Materials and methods

bEnd.3 cells (American Type Culture Collection, Manassas, VA, USA), an immortalized mouse cell line generated from brain capillary endothelial cells (Montesano et al., 1990) (within the passage 24–32), were grown in the culture medium of Dulbecco's modified Eagle's medium (DMEM; Gibco Invitrogen, Carlsbad, CA, USA) high glucose with 4.5 g/L D-glucose, L-glutamine and 110 mg/L sodium pyruvate, 10% fetal bovine serum (FBS), 100 U/mL penicillin, and 100 μg/mL streptomycin. HUVECs (Lonza, Walkersville, MD, USA) (passage of 2–7) were cultured in endothelial basal media (EBM-2; Lonza, Walkersville, MD, USA) supplemented with growth factors (EGM-2 SingleQuot Kits; Lonza, Walkersville, MD, USA). Cells were maintained in a humidified cell culture incubator at 37°C and 5% CO_2/95% air.

The cells were seeded in the inner-upper surface of a microchannel (μ-Slide $I^{0.4}$ Luer; Ibidi GmbH, Munich, Germany). The microchannel has an inner width (b) of 5mm, height (h) of

0.4mm, and length of 50mm. The overall height of the microchannel is 2mm and the thickness of the upper wall is 1.42mm. (The wall is made of a polyethylene derivative with a density of 0.93 g/cm^3 and a speed of sound 1950 m/s.) For static cultivation in the microchannel, cells were cultivated in a humidified cell culture incubator at 37°C and 5% CO_2/95% air and the culture medium was exchanged twice a day with fresh culture medium. The cells were cultivated for 5 days (37°C, 5% CO_2) to achieve 85% cell confluency before sonoporation experiment. Cultivation with shear stress was achieved using the set up shown in Fig. 1A. The microchannel was connected to a speed-controllable peristaltic pump (Cole-Parmer, Vernon Hills, IL, USA) with gas-permeable, platinum-cured silicone tubes (US Plastic Corp, Lima, OH, USA). A bubble trap was used to remove any bubbles in the circulating medium. The setup (Fig. 1A) was kept inside a temperature-controlled, water-jacketed CO_2 incubator. Fully developed laminar flow of complete culture medium (volumetric flow rate Q (ml/s)) was established in the microchannel to generate shear stress. The culture medium was exchanged twice a day with fresh culture medium. Cells within the microchannel were first subjected to 0.5 dyne/cm^2 for 4 hr and then 5 dyne/cm^2 ($\tau = 6\eta Q/b^2h$) for 5 days, simulating the *in vivo* shear stress condition in the veins and brain microvasculature (Desai et al., 2002). The viscosity (η) of the complete culture medium at 37°C for bEnd.3 cells was 0.00726 dyne·s/cm^2 and 0.00689 dyne·s/cm^2 for the medium for HUVECs, measured using a Schott Gerate viscometer (SI Analytics GmbH, Mainz, Germany).

For sonoporation experiment, the microchannel with seeded-cells under cultivation of flow or without flow was placed on a 37°C heating stage of an inverted microscope (Eclipse Ti-U, Nikon, Melville, NY, USA) (Fig. 1B). A planar US transducer (0.635 cm diameter, 1.25 MHz, Advanced Devices, Wakefield, MA, USA) driven by a function generator (33250A, Agilent Technologies, Palo Alto, CA, USA) and a 75 W power amplifier (75A250, Amplifier Research, Souderton, PA, USA) was used to generate US pulses. The transducer was calibrated in free field using a 40 μm calibrated needle hydrophone (HPM04/1, Precision Acoustics, Dorchester, UK). To minimize effects of reflection from interfaces of microchannel and water, short pulses (10 cycles) were used and the transducer was positioned at an angle of 45° with its active surface submerged in water ~ 7 mm (Rayleigh distance of the transducer) from the cells (inset in Fig. 1B). The spatial peak temporal peak negative pressure of 0.24MPa was used in our experiments. Since the acoustic impedance of the microchannel material (~1.78 × 10^6 Ns/m^{-3}) is close to that of water (1.48 × 10^6 Ns/m^{-3}), the effects of reflection and attenuation by the thin polyethylene derivative (~1.4mm) of microchannel is ignored (the pressure drop by the layer microchannel material is estimated to be less than 2%).To measure the $[Ca^{2+}]_i$, the cells were loaded with fura-2AM (Invitrogen, Carlsbad, CA, USA) before experiments. Complete culture medium (37°C) containing 5 μM fura-2AM dissolved in DMSO and 0.05% v/v of 10% w/v Pluronic F-127 (Invitrogen, Carlsbad, CA, USA) was added into the microchannel and incubated for 60 min. Excess dye was removed by washing the cells three times with Dulbecco's Phosphate-Buffered Saline solution (DPBS; 14040, Gibco Invitrogen, Carlsbad, CA, USA). The intercalating agent propidium iodide (PI) (Sigma Aldrich, St. Louis, MO, USA) was added before US application.

As described previously (Fan et al., 2010), dynamic multi-wavelength fluorescence imaging was performed to measure PI fluorescence and $[Ca^{2+}]_i$ concurrently using a cooled CCD camera (Photometrics QuantEM, Tucson, AZ, USA), a monochromator (DeltaRAM X™, PTI, Birmingham, NJ, USA) with 5 nm bandpass, which repeatedly filters light from a 75 W xenon lamp at 340, 380nm and 539nm, and a polychroic filter (73000v2, Chroma, Rockingham, VT, USA) for green and red. PI uptake in the cells was indicated by the increase of fluorescence at 610 nm (with 539 nm excitation). $[Ca^{2+}]_i$ values were obtained

from the ratio of the respective emission (510 nm) fluorescence intensities from 340 nm and 380 nm excitation (Grynkiewicz et al., 1985).

Definity™ microbubbles (Lantheus Medical Imaging, Billerca, MA, USA) (C_3F_8 gas core with a phospholipid shell, diameter 1.1 μm–3.3 μm) were used to provide a controllable agent to facilitate sonoporation. A high-speed camera (Fastcam SA1, Photron, San Diego, CA, USA) was used to capture US-driven microbubble activities (Fig. 1B).

As indicated in Fig. 1C, Definity™ (10^6 microbubbles/ml) and 120 μM PI in DPBS (extracellular calcium concentration, $[Ca^{2+}]_o$ = 0.9 mM) were added into the microchannel before the experiments, which were conducted without fluid flow. The microbubbles rose due to buoyancy and came into contact with the cells seeded on the inner upper surface of the microchannel. After recording of baseline fluorescence $[Ca^{2+}]_i$ and PI, bright field imaging (20,000 frames/s) was performed during an US tone burst (8 μs duration, 0.24 MPa peak negative pressure) (noted as t = 0 s), followed by fluorescence imaging up to 200 s.

Measurements were expressed as mean ± standard deviation. Statistical significance of detected differences between groups was tested using the unpaired Student's t-test (Version 16, SPSS, Chicago, IL, USA). The 2-sided P value was determined, testing the null hypothesis that the two population means are equal. The reported P-values for the t-tests were performed assuming equal variance between groups, except where Levene's test indicated likelihood of unequal variance ($P< 0.05$). P values less than 0.05 were considered to be statistically significant.

3. Results

The cells cultivated under shear stress exhibited orientation and elongation along the direction of the flow (along the length of the microchannel) compared with statistically cultured cells (Fig. 2). No change in either PI fluorescent intensity or $[Ca^{2+}]_i$ was detected for statically or shear stress cultivated cells without US application or with US but without microbubbles present. A total of 65 bEnd.3 cells from 8 independent experiments, including statically cultured cells (static groups, n=32) and shear stress cultured cells (shear stress group, n=33), were examined to obtain intracellular PI uptake and $[Ca^{2+}]_i$ changes after US application. A total of 74 HUVECs, (static group n=30; shear stress group n=44) from 9 independent experiments were examined. Each of the cells examined had a microbubble in direct contact with the cell membrane in a similar configuration, and fragmented or shrunk due to the US exposure.

Figure 3 shows the typical results of PI and $[Ca^{2+}]_i$ changes in bEnd.3 cells. The enlarged views of the bright field images of the microbubbles (Figs. 3A and 3D) showing shrinkage (Fig. 3A) or fragmentation (Fig. 3D) confirmed the US effect on the microbubble, although the detail process of microbubble oscillation or collapse driven by the 1.25 MHz US pulse was not captured at the imaging frame rate (20,000 frames/s) used in the experiment. The absence of PI fluorescence (top image in Figs. 3B and 3E) and the constant initial $[Ca^{2+}]_i$ values (top image in Figs. 3C and 3F) before US indicated the intact membrane.

In the statically cultured cell, the increase of PI intensity and $[Ca^{2+}]_i$ (Figs. 3B and 3C) initiated from the membrane location in contact with the microbubble and then spread within the cell. The mean PI fluorescence intensities within the cells (Figs. 3B and 3G) in the statically cultured cell increased significantly to a stable value after US application, while no change was detected in the shear stress cultured cell (Figs. 3E and 3G). The PI fluorescence increased when the PI molecules entered the cell via the membrane disruption and bound to the RNA in the cytoplasm and/or the DNA in the nucleus. Hence the PI could be used as a marker for reversible permeabilization of the cell membrane (van Wamel et al., 2006). The

limited, transient increase of PI fluorescence suggests temporary permeation generated by the microbubble and resealing of the cell membrane after US (Deng et al., 2004; Kudo et al., 2009; Mehier-Humbert et al., 2005). The cells showing limited, transient increase of PI fluorescence was confirmed of their viability using Trypan blue assay.

The mean values of $[Ca^{2+}]_i$ also increased in the statically cultured cell, reaching its maximum before recovering (Fig. 3H). In contrast, the shear cultivated bEnd.3 cell exhibited no change in either PI fluorescence intensity or $[Ca^{2+}]_i$ (Figs. 3G and 3H).

Overall, cells in the shear stress groups exhibited much less responses to the impact of the US-driven microbubbles than cells in the static groups, as indicated by Fig. 3 and the data in Tables 1 and 2. Both bEnd.3 cells and HUVECs in the shear stress group exhibited less increases of PI (Table 1) and $[Ca^{2+}]_i$ (Table 2). The percentages of cells with PI uptake and $[Ca^{2+}]_i$ changes in the shear stress group are also much lower (Figs. 4A and 4B, Tables 1 and 2). (The percentages were calculated based on the following criteria: the maximum fluorescence intensity value after US is at least 2σ greater than the averaged value before US, where σ is the standard deviation of the measured values before US). The data indicate that bEnd.3 cells and HUVECs exhibited similar characteristics in terms of these responses.

In addition to the immediate $[Ca^{2+}]_i$ changes observed in the individual cells that were directly in contact with microbubbles, calcium wave, or the subsequent changes of $[Ca^{2+}]_i$ in the surrounding cells was also observed in this study. In the statically cultured monolayer of HUVECs (Fig. 5A), the initial values of $[Ca^{2+}]_i$ before US were lower than in the shear cultured cells (Fig. 5B). In each case, the calcium wave was initiated from a cell that was adjacent to microbubble (top image in Figs. 5A and 5B) and that exhibited immediate change in $[Ca^{2+}]_i$ after US (images at 2s in Figs. 5A and 5B). The extent of the calcium wave, represented by the area within which the cells exhibited delayed $[Ca^{2+}]_i$ changes, was larger in the statically cultured monolayer than in the shear cultured monolayer (Fig. 5C). For example, the area was about 3 times larger in the statically cultured monolayer at 11s after US.

4. Discussion

This study examined sonoporation of cells that were cultured under constant shear stress of 5 dyne/cm^2 for 5 days to simulate the *in vivo* shear stress condition in the microvasculatures which has a range of 4-20 dyne/cm^2 (Desai et al., 2002). Higher shear stress may result in more pronounced differences compared with statically cultured cells, but the exact dependence remains to be investigated.

Shear stress on endothelial cells is likely to be translated into biological responses by interactions among the cytoskeleton, ion channels, and membrane receptors (Davies, 1995), thereby activating a chain of biochemical and genetic processes that allow the cells to adapt to flow. Although the exact mechanism requires further investigation, the observed reduced response in terms of membrane disruption and changes in $[Ca^{2+}]_i$ in shear stress cultivated endothelial cells may be attributed to the shear induced changes in biomechanical and cellular properties of endothelial cells, particularly the significant increase in intracellular viscoelasticity and intracellular cytoplasmic stiffening (Icard-Arcizet et al., 2008; Lee et al., 2006; Wang and Ingber, 1994). These biomechanical adaptations may result in higher resistance in these cells to US-driven microbubble activities (O'Brien, 2007) compared to cells cultured in static condition. The cell-cell interactions could also be affected, resulting in the reduced extent of $[Ca^{2+}]_i$ waves observed in shear stress cultured cells.

The observation that more cells had changes in $[Ca^{2+}]_i$ than had PI uptake (Fig. 4), indicate that US generated change of $[Ca^{2+}]_i$ without causing membrane disruption in some cases.

This could happen if the disruption was too small to allow enough PI into the cells to be detectable under the current experimental setting. However, US-driven microbubbles can also induce $[Ca^{2+}]_i$ changes via mechanisms other than membrane disruption. For example, activation of stretch activated channels (SACs) in endothelial cells could induce Ca^{2+} influx followed by Ca^{2+} release from internal stores (Tran et al., 2008;Tran et al., 2007) without membrane disruption.

The sonoporation experiments in this study were conducted without flow in the microchannel to avoid its effects for the static groups, and the influence of on-going flow was not included. As the cells most likely already reached a steady state of adaptation after 5 days cultivation under shear stress, the on-going flow may not have additional significant effect on the state of the cells. Even with flow present, the relative slow flow velocity compared to US propagation velocity (1500 m/s) and frequency (1.25 MHz) are not expected to affect US-driven microbubble activities and sonoporation. However, on-going flow may affect the exact patterns of $[Ca^{2+}]_i$ waves, since $[Ca^{2+}]_i$ waves depend on the propagation of intercellular or extracellular messengers such as IP_3 from cell to cell (Sanderson, 1996; Sanderson et al., 1994) and ATP (Cotrina et al., 1998; Osipchuk and Cahalan, 1992).

The US exposure parameters in this study were chosen to ensure high cell viability and produce detectable effects. The effects of other US conditions on the reduced response to US are not included, although the basic characteristics of the observed phenomena are expected to remain similar.

In conclusion, this study revealed that shear stress cultivation results in reduced responses in bEnd.3 cells and HUVECs to the impact of US-driven microbubble activities in terms of cell membrane permeability and $[Ca^{2+}]_i$ dynamics. These differences are important in translating results from *in vitro* sonoporation studies to *in vivo* environments in the development of US techniques for drug and gene delivery. Considering the important regulatory role Ca^{2+} plays in physiological and pathological processes such as gene transcription, cell proliferation, metabolism, cell migration, and wound response (Berridge et al., 2003; Petty, 2006), these results may also be relevant for endothelial cell biology and other bioengineering applications.

However, beyond the obvious steps to extend the current study to examine a wider range of US exposure conditions and shear stress values, probably more importantly, the detail processes and molecular mechanisms of US induced cell responses need to be investigated to fully understand the effect shear stress on sonoporation of cells. It is well known that US driven microbubbles generate mechanical impact via mechanical pressure and fluid movement, but it is unclear how cells respond to these mechanical inputs and stimuli fundamentally, e.g., the detail cellular pathways and molecular processes involved in the cell responses to US are unknown.

Acknowledgments

This work is support in part by the U. S. National Institutes of Health (R01CA116592 to C. X. Deng). We thank Chulwoo Jung for his assistance on the viscosity measurements.

References

Abbott, NJ. Role of intracellular calcium in regulation of brain endothelial permeability.. In: Pardridge, WM., editor. “Introduction to the blood-brain barrier: Methodology, biology and pathology. Cambridge University Press; New York: 1998. p. 345-351.

Barbee KA, Davies PF, Lal R. Shear stress-induced reorganization of the surface topography of living endothelial cells imaged by atomic force microscopy. Circ. Res. 1994; 74(1):163–171. [PubMed: 8261591]

Berridge MJ, Bootman MD, Roderick HL. Calcium signalling: dynamics, homeostasis and remodelling. Nat Rev Mol Cell Biol. 2003; 4(7):517–29. [PubMed: 12838335]

Bradbury MW. The blood-brain barrier. Experimental Physiology. 1993; 78(4):453–472. [PubMed: 8398100]

Brown RC, Davis TP. Calcium modulation of adherens and tight junction function: A potential mechanism for blood-brain barrier disruption after stroke. Stroke. 2002; 33(6):1706–1711. [PubMed: 12053015]

Cotrina ML, Lin JHC, Nedergaard M. Cytoskeletal assembly and ATP release regulate astrocytic calcium signaling. J. Neurosci. 1998; 18(21):8794–8804. [PubMed: 9786986]

Dardik A, Liu A, Ballermann BJ. Chronic in vitro shear stress stimulates endothelial cell retention on prosthetic vascular grafts and reduces subsequent in vivo neointimal thickness. Journal of Vascular Surgery. 1999; 29(1):157–167. [PubMed: 9882800]

Davies PF. Flow-mediated endothelial mechanotransduction. Physiol Rev. 1995; 75(3):519–560. [PubMed: 7624393]

Deng C, Sieling F, Pan H, Cui J. Ultrasound-induced cell membrane porosity. Ultrasound Med Biol. 2004; 30(4):519–526. [PubMed: 15121254]

Desai SY, Marroni M, Cucullo L, Krizanac-Bengez L, Mayberg MR, Hossain MT, Grant GG, Janigro D. Mechanisms of endothelial survival under shear stress. Endothelium. 2002; 9:89–102. [PubMed: 12200960]

Eliasson L, Proks P, Ammala C, Ashcroft FM, Bokvist K, Renstrom E, Rorsman P, Smith PA. Endocytosis of secretory granules in mouse pancreatic beta-cells evoked by transient elevation of cytosolic calcium. J Physiol. 1996; 493(Pt 3):755–767. [PubMed: 8799897]

Fan Z, Kumon RE, Park J, Deng CX. Intracellular delivery and calcium transients generated in sonoporation facilitated by microbubbles. Journal of Controlled Release. 2010; 142:31–39. [PubMed: 19818371]

Garcia-Cardena G, Comander J, Anderson KR, Blackman BR, Gimbrone MA. Biomechanical activation of vascular endothelium as a determinant of its functional phenotype. Proc Natl Acad Sci. 2001; 98(8):4478–4485. [PubMed: 11296290]

Girard PR, Nerem RM. Shear stress modulates endothelial cell morphology and F-actin organization through the regulation of focal adhesion-associated proteins. Journal of Cellular Physiology. 1995; 163(1):179–193. [PubMed: 7534769]

Grynkiewicz G, Poenie M, Tsien RY. A new generation of Ca^{2+} indicators with greatly improved fluorescence properties. J Biol Chem. 1985; 260(6):3440–50. [PubMed: 3838314]

Hariri R. Cerebral oedema. Neurosurg Clin North Am. 1994; 5(4):687–706.

Icard-Arcizet D, Cardoso O, Richert A, Henon S. Cell stiffening in response to external stress is correlated to actin recruitment. Biophysical Journal. 2008; 94(7):2906–2913. [PubMed: 18178644]

Juffermans LJ, Dijkmans PA, Musters RJ, Visser CA, Kamp O. Transient permeabilization of cell membranes by ultrasound-exposed microbubbles is related to formation of hydrogen peroxide. Am J Physiol Heart Circ Physiol. 2006; 291(4):H1595–601. [PubMed: 16632548]

Kudo N, Okada K, Yamamoto K. Sonoporation by single-shot pulsed ultrasound with microbubbles adjacent to cells. Biophysical Journal. 2009; 96(12):4866–4876. [PubMed: 19527645]

Kumon RE, Aehle M, Sabens D, Parikh P, Han YW, Kourennyi D, Deng CX. Spatiotemporal effects of sonoporation measured by real-time calcium imaging. Ultrasound Med Biol. 2009; 35:494–506. [PubMed: 19010589]

Kumon RE, Aehle M, Sabens D, Parikh P, Kourennyi D, Deng CX. Ultrasound-induced calcium oscillations and waves in Chinese hamster ovary cells in the presence of microbubbles. Biophys J. 2007; 93(6):L29–31. [PubMed: 17631537]

Langille B, Graham J, Kim D, Gotlieb A. Dynamics of shear-induced redistribution of F-actin in endothelial cells in vivo. Arterioscler Thromb Vasc Biol. 1991; 11:1814–1820.

Lee JSH, Panorchan P, Hale CM, Khatau SB, Kole TP, Tseng Y, Wirtz D. Ballistic intracellular nanorheology reveals ROCK-hard cytoplasmic stiffening response to fluid flow. Journal of Cell Science. 2006; 119(9):1760–1768. [PubMed: 16636071]

Lionetti V, Fittipaldi A, Agostini S, Giacca M, Recchia FA, Picano E. Enhanced caveolae-mediated endocytosis by diagnostic ultrasound in vitro. Ultrasound in Medicine & Biology. 2009; 35(1): 136–143. [PubMed: 18950933]

MacDonald PE, Eliasson L, Rorsman P. Calcium increases endocytotic vesicle size and accelerates membrane fission in insulin-secreting INS-1 cells. J. Cell Sci. 2005; 118(24):5911–5920. [PubMed: 16317049]

Malek AM, Izumo S. Mechanism of endothelial cell shape change and cytoskeletal remodeling in response to fluid shear stress. Journal of Cell Science. 1996; 109(4):713–726. [PubMed: 8718663]

Mayer CR, Geis NA, Katus HA, Bekeredjian R. Ultrasound targeted microbubble destruction for drug and gene delivery. Export Opinion on Drug Delivery. 2008; 6(7):745–768.

Mehier-Humbert S, Bettinger T, Yan F, Guy RH. Plasma membrane poration induced by ultrasound exposure: Implication for drug delivery. Journal of Controlled Release. 2005; 104(1):213–222. [PubMed: 15866347]

Montesano R, Pepper MS, Mohle-Steinlein U, Risau W, Wagner EF, Orci L. Increased proteolytic activity is responsible for the aberrant morphogenetic behavior of endothelial cells expressing the middle T oncogene. Cell. 1990; 62(3):435–45. [PubMed: 2379237]

Morita T, Kurihara H, Maemura K, Yoshizumi M, Yazaki Y. Disruption of cytoskeletal structures mediates shear stress-induced endothelin-1 gene expression in cultured porcine aortic endothelial cells. The Journal of Clinical Investigation. 1993; 92(4):1706–1712. [PubMed: 8408624]

O'Brien JWD. Ultrasound-biophysics mechanisms. Progress in Biophysics and Molecular Biology. 2007; 93(1-3):212–255. [PubMed: 16934858]

Ohl C-D, Arora M, Ikink R, de Jong N, Versluis M, Delius M, Lohse D. Sonoporation from jetting cavitation bubbles. Biophysical Journal. 2006; 91(11):4285–4295. [PubMed: 16950843]

Olesen S. An electrophysiological study of microvascular permeability and its modulation by chemical mediators. Acta Physiol Scand. 1989; 136(Suppl. 579):1–28. [PubMed: 2773653]

Osipchuk Y, Cahalan M. Cell-to-cell spread of calcium signals mediated by ATP receptores in mast cells. Nature. 1992; 359(6392):241–244. [PubMed: 1388246]

Petty HR. Spatiotemporal chemical dynamics in living cells: from information trafficking to cell physiology. Biosystems. 2006; 83(2-3):217–24. [PubMed: 16236427]

Postema M, van Wamel A, Lanc CT, de Jong N. Ultrasound-induced encapsulated microbubble phenomena. Ultrasound in Medicine & Biology. 2004; 30(6):827–840. [PubMed: 15219962]

Prentice P, Cuschieri A, Dholakia K, Prausnitz M, Campbell P. Membrane disruption by optically controlled microbubble cavitation. Nature Physics. 2005; 1(2):107–110.

Sanderson M. Intercellular waves of communication. Nes Physiol Sci. 1996; 11:262–269.

Sanderson M, Charles A, Boitano S, Dirksen E. Mechanisms and function of intercellular calcium signaling. Mol Cell Endocrinol. 1994; 98:173–187. [PubMed: 8143927]

Tran TA, Le Guennec JY, Bougnoux P, Tranquart F, Bouakaz A. Characterization of cell membrane response to ultrasound activated microbubbles. Ultrasonics, Ferroelectrics and Frequency Control. IEEE Transactions on. 2008; 55(1):43–49.

Tran TA, Roger S, Le Guennec JY, Tranquart F, Bouakaz A. Effect of ultrasound-activated microbubbles on the cell electrophysiological properties. Ultrasound in Medicine & Biology. 2007; 33(1):158–163. [PubMed: 17189059]

Tsukamoto, A.; Yasui, N.; Watanabe, Y.; Furukawa, K.; Ushida, T. Real-time imaging of interaction between microbubble and cell under therapeutic ultrasound radiation.. In: Hierlemann, A., editor. Sixth IASTED International Conference. Acta Press; Innsbruck, Austria: 2008. p. 334-337.

van Wamel A, Kooimana K, Hartevelda M, Emmera M, ten Catec FJ, Versluisd M, de Jonga N. Vibrating microbubbles poking individual cells: Drug transfer into cells via sonoporation. Journal of Controlled Release. 2006; 112(2):149–155. [PubMed: 16556469]

VanBavel E. Effects of shear stress on endothelial cells: Possible relevance for ultrasound applications. Progress in Biophysics and Molecular Biology. 2007; 93(1-3):374–383. [PubMed: 16970981]

Wang N, Ingber DE. Control of cytoskeletal mechanics by extracellular matrix, cell shape, and mechanical tension. Biophysical Journal. 1994; 66(6):2181–2189. [PubMed: 8075352]

Wu J. Shear stress in cells generated by ultrasound. Progress in Biophysics and Molecular Biology. 2007; 93(1-3):363–373. [PubMed: 16928394]

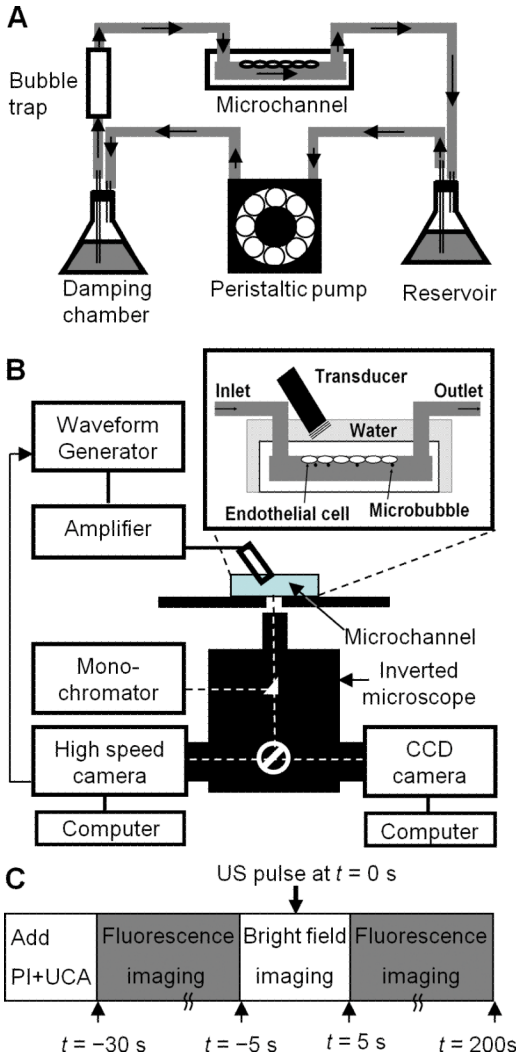

Figure 1.

Experimental setup and procedures. (A) Shear stress cultivation of endothelial cells in a microchannel. Placed inside a humidified cell culture incubator with gas supply (5% CO_2-95% air), the cells were cultured on the inner-upper surface of the microchannel which was connected to a continuous flow circuit of complete culture medium. (B) Sonoporation setup with real-time fluorescence imaging and high-speed bright field imaging. (C) Experimental procedures involving bright field and fluorescence imaging of microbubble activities and sonoporation.

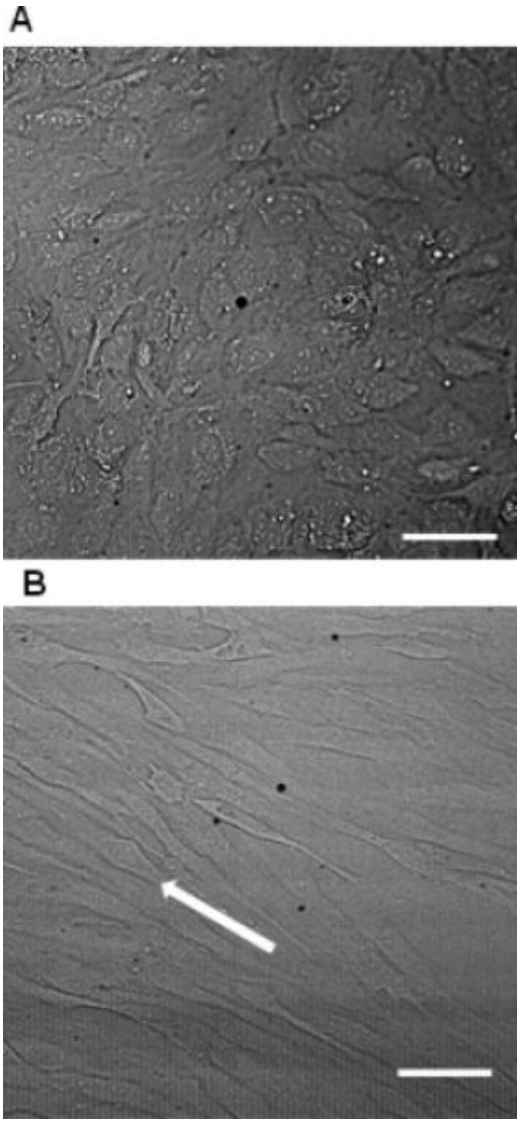

Figure 2.
Representative HUVEC cell morphology of static cultivation (A) and shear stress cultivation (B). The cells cultivated under 5 dyne/cm^2 for 5 day exhibited orientation and elongation along the direction of the flow (arrow in B). The scale bars represent 100 μm.

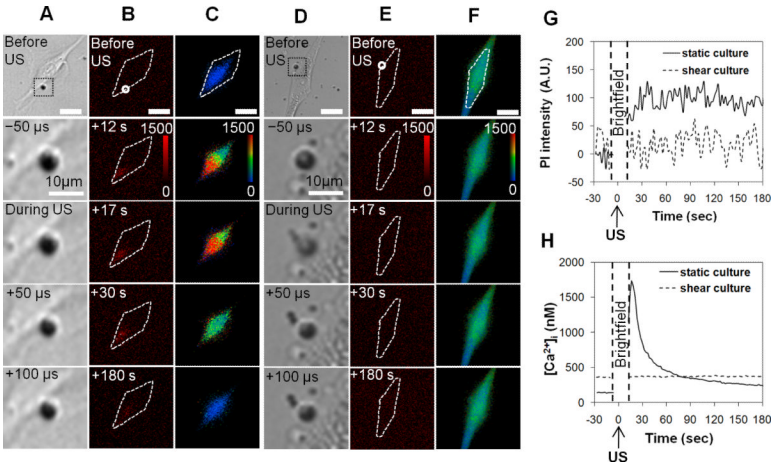

Figure 3.

Representative results of PI uptake and $[Ca^{2+}]_i$ changes in bEnd.3 cells from the static group (A-C) and shear stress group (D-F) generated by US stimulated microbubbles. Panels (A) and (D) show the high speed brightfield imaging of a microbubble near the cell membrane with enlarged views before, during, and after the US exposure which started at t=0 s. Panels (B) and (C) show the time-lapse images of PI fluorescence and $[Ca^{2+}]_i$ in the statically cultured cell. Panels (E) and (F) the time-lapse images of PI fluorescence and $[Ca^{2+}]_i$ images for the shear stress cultured cell. The color bars in (B) and (E) indicate the PI intensity in arbitrary units (A. U.) and in (C) and (F) indicate $[Ca^{2+}]_i$ in nM. The scale bars represent 25 μm.

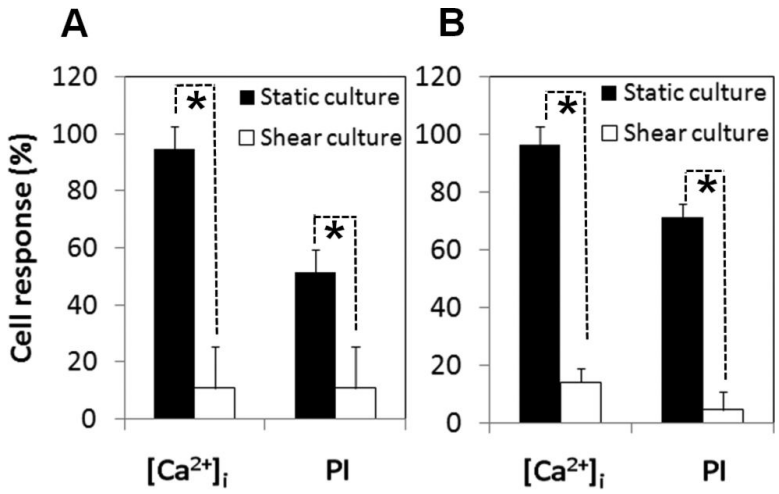

Figure 4.

Shear stress cultured cells exhibited different response to US application from the statically cultured cells. (A) Shear stress cultured bEnd.3 cells (n = 33) exhibited lower percentage of responses in PI uptake and $[Ca^{2+}]_i$ changes compared with the static group (n = 32). (B) Shear stress cultured HUVECs (n = 44) had lower percentages of responses compared with the static group (n = 30). The asterisk indicates $P < 0.05$ for a Student's t-test between cells in the static and shear stress group.

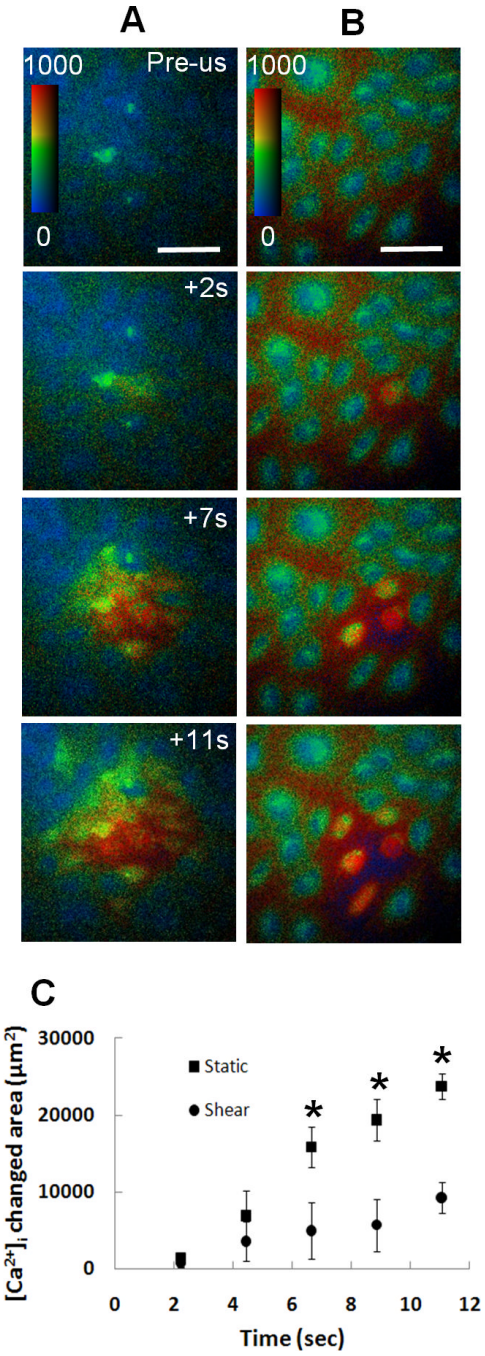

Figure 5.

US-induced calcium wave in shear stress cultured monolayer of HUVECs was reduced compared with the statically cultured cells. (A) $[Ca^{2+}]_i$ wave in statically cultivated monolayer shown as the increasing area within which cells exhibited $[Ca^{2+}]_i$ changes. (B) $[Ca^{2+}]_i$ wave in shear stress cultivated monolayer.The color bars indicate $[Ca^{2+}]_i$ in nM. The scale bars represent 100 μm. (C) The area within which cells exhibiting changes in $[Ca^{2+}]_i$ for static (n=5) and shear stress cultivated monolayer (n=5). The asterisk indicates $P < 0.05$ for a Student's *t*-test between the shear stress cultured cells and the statically cultured cells.

Table 1

US-induced changes of PI fluorescence intensity

	Static group		Shear stress group	
	Percentage of cells with increase (%)	**Maximum increase (A.U.)**	**Percentage of cells with increase (%)**	**Maximum increase (A.U.)**
b.End3 cells	51.3 ± 8.3 (n=32)	69 ± 97 (n=32)	10.7 ± 14.7 (n=33)	6.0 ± 27 (n=33)
HUVECs	70.9 ± 10.5 (n=30)	148 ± 153 (n=30)	4.4 ± 6.1 (n=44)	25 ± 56 (n=44)

Table 2

US induced changes of $[Ca^{2+}]_i$

	Static group		Shear stress group	
	Percentage of cells with increase (%)	**Maximum increase (nM)**	**Percentage of cells with increase (%)**	**Maximum increase (nM)**
b.End3 cells	94.6 ± 7.7 (n=32)	611 ± 408 (n=32)	10.7 ± 14.7 (n=33)	63 ± 164 (n=33)
HUVECs	96.4 ± 7.1 (n=30)	658 ± 388 (n=30)	13.9 ± 4.8 (n=44)	81 ± 148 (n=44)